Journal of
Synchrotron
Radiation

ISSN 0909-0495

Received 28 March 2012
Accepted 30 September 2012

Time-resolved XAS (Bonn-SUT-SLRI) beamline at SLRI

Yingyot Poo-arporn,[a] Prae Chirawatkul,[a] Worasarit Saengsui,[b] Siwarak Chotiwan,[c] Sutasinee Kityakarn,[c] Supat Klinkhieo,[a] Josef Hormes[d] and Prayoon Songsiriritthigul[a,e]*

[a]Synchrotron Light Research Institute, Nakhon Ratchasima 30000, Thailand, [b]Nanomaterials Science Program, Faculty of Science, Kasetsart University, Bangkok 10903, Thailand, [c]Department of Chemistry, Faculty of Science, Kasetsart University, Bangkok 10903, Thailand, [d]Canadian Light Source, University of Saskatchewan, 101 Perimeter Road, Saskatoon, SK, Canada S7N OX4, and [e]School of Physics, Suranaree University of Technology, Nakhon Ratchasima 30000, Thailand. E-mail: prayoon@slri.or.th

An energy-dispersive X-ray absorption spectroscopy beamline has been constructed at the Synchrotron Light Research Institute, Thailand. The beamline was designed to utilize the synchrotron radiation with photon energies between 2400 and 8000 eV. The horizontal focusing of the bent crystal in the energy-dispersive monochromator offers a small polychromatic focal spot of 1 mm at the sample position. By employing an energy-dispersive scheme, the whole X-ray absorption near-edge structure (XANES) can be obtained simultaneously using a position-sensitive detector with a fastest readout speed of 25 ms. The short data collection time opens a new opportunity for time-resolved X-ray absorption spectroscopy (XAS) experiments such as studies of changes of the electronic structures or the local coordination environments of an atom during a change in thermodynamic conditions. For this purpose, an *in situ* cell was designed and fabricated for the beamline. Thermal oxidation of TiO_2 was chosen as an *in situ* experiment example. The structural change of TiO_2 as a function of temperatures was monitored from the change in the measured XAS spectra. The obtained Ti *K*-edge XANES spectra clearly show the formation of an anatase phase when the temperature was raised to 673 K.

Keywords: time-resolved XAS; energy dispersive; *in situ* measurement; TiO_2.

1. Introduction

X-ray absorption spectroscopy (XAS) has been widely used to determine valance states or local structures of various materials (Koningsberger & Prins, 1988; Hedman & Pianetta, 2007; Bunker, 2010, and references therein). In a conventional XAS set-up an XAS spectrum measurement involves a mechanical scanning of a double-crystal monochromator (DCM). This limits the data acquisition time to several minutes. Thus, it is not possible to monitor rapid changes of local structures or valence states of some processes such as the change in the valence state of Fe(III) porphyrin during a photoinduced electron transfer (Chen *et al.*, 1999) and the change of Fe neighboring atoms during a dissociation of ferrioxalate (Chen *et al.*, 2007), processes that take place within 10 ms and 115 ps, respectively. To overcome this problem, two schemes to increase the data collection speed have been proposed. For the first scheme, called the quick-scanning EXAFS (QEXAFS), a typical DCM is replaced by a piezo-driven (Lützenkirchen-Hecht *et al.*, 2001) or a cam-driven DCM (Caliebe *et al.*, 2006) and an XAS spectrum can be measured in milliseconds. The second scheme is to use an energy-dispersive set-up (Flank *et al.*, 1983; Blank *et al.*, 1992; Pascarelli *et al.*, 1999; Cezar *et al.*, 2010), which allows the whole XANES spectrum to be measured simultaneously, and the data collection speed is mainly limited by the electronics of the detector which is typically in the range of a millisecond or microsecond.

2. Energy-dispersive set-up

In an energy-dispersive XAS (EDXAS) set-up a bent crystal is employed to disperse and focus X-rays with a continuous band of photon energies. Fig. 1 shows a schematic diagram for the EDXAS set-up. For simplicity, it may be considered that the crystal is bent to a cylindrical shape with a radius of curvature R. The relation between the source-to-crystal distance (p) and the crystal-to-focus distance (q) for the bent crystal follows an equation for cylindrical optics, which is

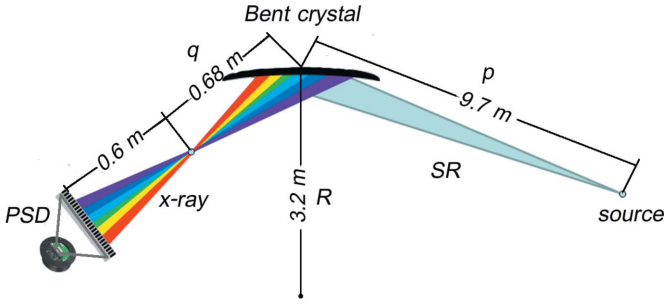

Figure 1
Optical layout for an EDXAS scheme. X-rays with a certain energy bandwidth are selected by a bent crystal. The selected X-rays are focused at the sample position. The position-sensitive detector (PSD) is placed downstream of the sample to detect all the transmitted X-rays simultaneously thus allowing the measurement of an XAS spectrum in a short period of time.

$$(1/p) + (1/q) = 2/(R \sin\theta), \qquad (1)$$

where θ is the Bragg angle. At a certain Bragg angle the usable energy range is given by

$$\Delta E = E \cot\theta \Delta\theta = E \cot\theta\{(l/R) - [(l \sin\theta)/p]\}, \qquad (2)$$

where l is an illuminated length on the crystal and $\Delta\theta$ is a range of incident angles with respect to the crystal surface.

Using the energy-dispersive scheme, XAS spectra can be obtained with less vibration-induced noise compared with the conventional set-up as there are no mechanical movements during the measurements, the beam size at the sample position can be small which allows small samples to be measured, and a good output-linearity and a wide dynamic range of a position-sensitive detector (PSD) gives good signal-to-noise ratio data and a fast detection speed (Fontaine *et al.*, 1987). A number of researches have been made using the EDXAS set-up. These include the study of the $Cu^{2+} \rightarrow Cu^{+}$ transformation in a cathodic reduction of Cu in conductive polymers (Dartyge *et al.*, 1986) where Cu *K*-edge XANES spectra were measured every 7.2 s, the investigation of a thermal dehydration process in a Ni^{2+} ion exchanged zeolite Y (Couves *et al.*, 1990) using Ni *K*-edge XANES, and the crystallization of some nanomaterials (Meneses *et al.*, 2006).

3. TRXAS beamline

The time-resolved XAS (TRXAS) beamline is designed to utilize synchrotron radiation generated from a bending magnet of a 1.2 GeV storage ring of the Siam Photon Source. It employs an energy-dispersive monochromator (EDM) and a 2θ arm with an angular range from 20 to 140° which were donated by the University of Bonn, Germany. The components belonged to a decommissioned beamline at the Electron Stretcher and Accelerator (ELSA) of the University of Bonn (Blank *et al.*, 1992). With a Si(111) crystal, the EDM covers photon energies between 2400 and 8000 eV, allowing the *K*-edges of S to Co to be investigated at this beamline. The rest of the beamline components were designed and fabricated in-house.

Because of the requirement for low-energy X-rays, no Be window was used to separate the vacuum between the storage ring and the beamline. Instead, a pressure-reduction tube was installed to connect the ultra-high-vacuum level (2×10^{-10} torr) at the front-end to a high vacuum level (1×10^{-6} torr) in the EDM (Fig. 2). However, since there is no cooling to the bent crystal in the EDM, a water-cooled 25 µm-thick Be foil was placed upstream of the EDM to reduce the heat load dissipated on the crystal from the white-beam radiation. Without the Be foil, the power dissipating on the crystal is about 4.7 W at 100 mA of stored beam. When the Be foil is inserted into the optical path, about 60% of the power is absorbed by the foil. The reduction of the photon flux owing to the Be foil measured by an ionization chamber was 5% at 5 keV photon energy. The reduction of the photon flux is higher at lower photon energies. Thus, the Be foil is installed on a linear drive, allowing the Be foil to be retracted from the optical line when measuring *K*-edge absorption spectra of light elements such as sulfur. Upstream of the EDM there are

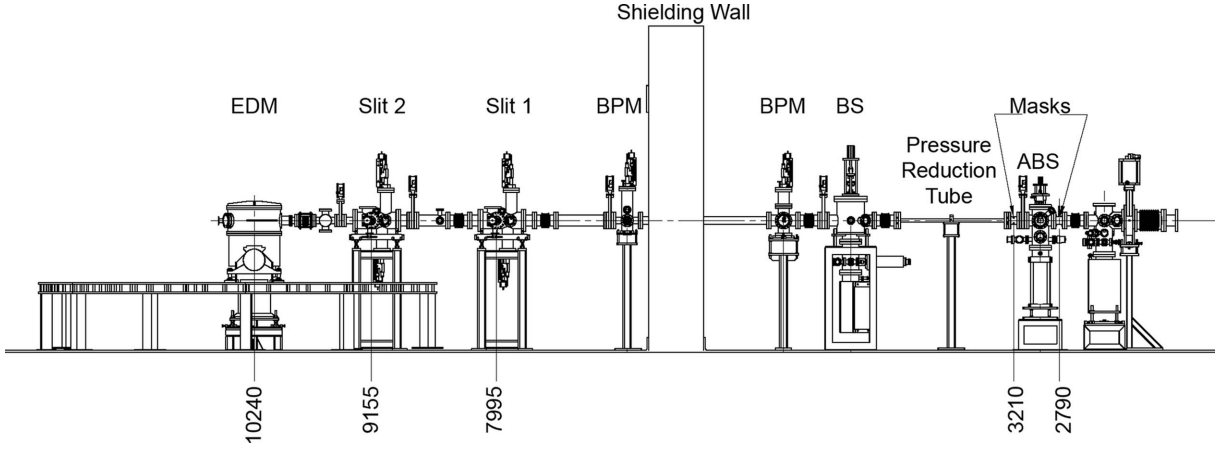

Figure 2
Schematic of the TRXAS beamline showing the main components, namely the heat absorber (ABS), front-end masks, differential pressure tube, beam shutter (BS), retractable water-cooled Be foil, beam-position monitor (BPM), two sets of horizontal and vertical slits and EDM. Distances from the source (in mm) are also shown.

four pairs of water-cooled slits used to adjust the size of the beam entering the EDM and two wire-type photon beam position monitors to determine the profile of the beam horizontally and vertically.

The rectangular-shape Si(111) crystal with an area of 25 mm × 250 mm and a thickness of 1 mm was used as a bent crystal. The elliptical curvature of the crystal is adjustable using a crystal bender which is mounted on a three-axis goniometer placed inside the monochromator chamber. The goniometer allows the crystal to be rotated around three axes and translated vertically. The axes of rotation are the vertical axis, the axis normal to the crystal surface, and the axis along the length of the crystal. The distance between the center of the crystal and the source point is 9.7 m. This distance was set to be as short as possible for a high photon flux and a large acceptance angle on the bent crystal. At 9.7 m from the source the largest horizontal acceptance angle is 5 mrad.

Fig. 3 shows the end-station of the TRXAS beamline. The end-station is on the 2θ arm which can be rotated to satisfy the Bragg condition. As the focusing position along the arm can be varied, the end-station can also be translated such that the sample is always at the focusing position. The shortest crystal-to-focus distance available for the current set-up is about 0.6 m. The end-station is kept under a rough vacuum level of 2×10^{-2} torr and each section is separated by circular Kapton windows of outer diameter 15 mm and thickness 7.5 µm. Technically, the Kapton window can be replaced with a polypropylene window if higher photon flux at the sample position is required.

A PSD generally consists of a multi-element photodiode array which converts incoming electromagnetic radiation into a recordable signal such as a current or a voltage using the photoelectric effect (Tassell & Maule, 1979). The PSD at the TRXAS beamline is a commercially available NMOS linear image sensor model S3904-1024N from the Hamamatsu Company. The photodiode array contains 1024 elements each with an n-type diffusion layer formed on a p-type silicon substrate as a p–n junction and an active area of 20 µm × 2.5 mm. This detector uses a charge integration method to collect a signal. The generated electrical charges are temporarily stored in the junction capacitance of each photodiode and subsequently read out through the video line. After the detector is initiated by a start-pulse input, the signals are read out from each photodiode in sequence. The fastest readout frequency of the S3904-1024 model is 50 kHz. Thus, with 1024 photodiodes, the minimum time for the signal to be read out is 24 µs × 1024 = 24.58 ms. Hence, the fastest detection speed for this model is set to be 25 ms. The advantage of this data collection procedure is that the intensity of the signal output depends on the integration time which can be increased for low-light-level detection. However, as the charge-storage capacity is limited, the signal output will not increase if the intensity of the light is higher than the saturation level of the detector. The maximum storage charge capacitance for this model is 25 pC.

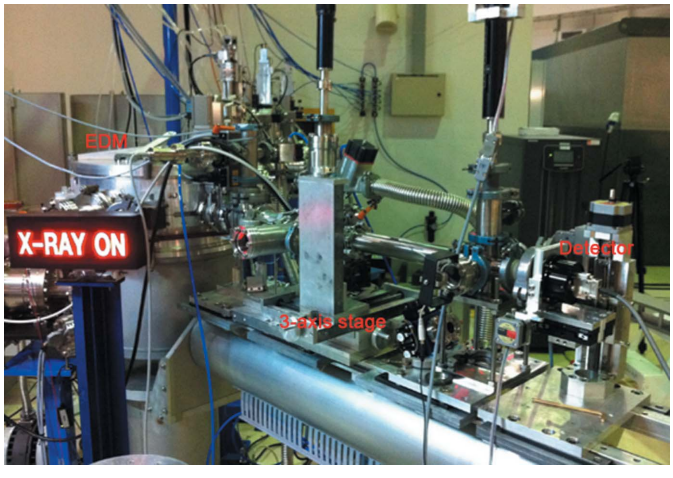

Figure 3
Photograph of the TRXAS end-station showing, from left to right, the EDM, three-axis stage and 1024-channel NMOS linear image sensor.

4. Commissioning results and performance test

4.1. Beamline commissioning

The radius of curvature for the Si(111) bent crystal can be estimated experimentally. As the p value is fixed at 9.7 m, the q value for a given θ was determined from the measured position of the focal spot. Thus the radius of curvature can be calculated using equation (1). For the set-up for Ti K-edge measurements, as an example, the maximum bending radius is 3.2 m with the corresponding crystal-to-focus distance and Bragg angle of 68.5 cm and 23.32°, respectively.

Fig. 4 demonstrates the useful photon energy range of the beamline. It covers photon energy for measuring a K-edge XANES spectrum from sulfur to iron. The XANES spectra in the figure were taken from S_8 powder and a 5 µm-thick Fe foil. A thin layer of S_8 powder was spread on a Kapton tape for the XANES measurement. In the set-up for measuring the S K-

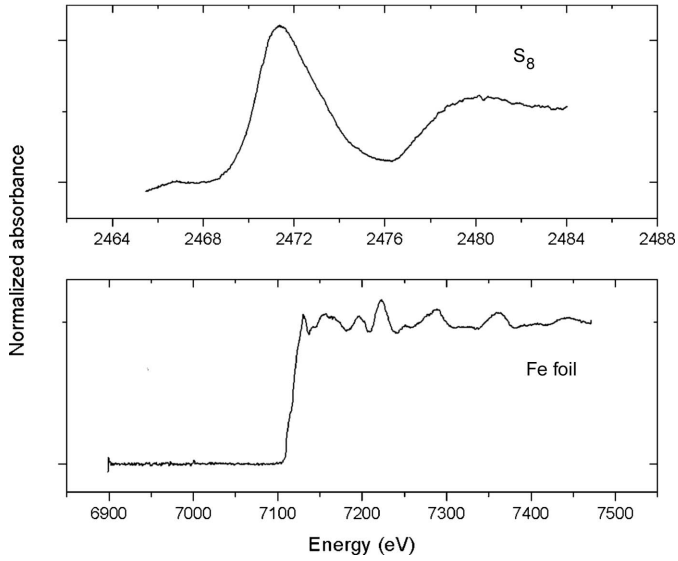

Figure 4
Normalized Fe K-edge XANES spectrum for a 5 µm-thick Fe foil and a normalized S K-edge XANES spectrum for S_8.

edge XANES spectrum the focal point of the photon beam is about 155 cm from the crystal. To avoid the loss of photon flux in this low-energy region the sample was measured under a 2×10^{-2} torr vacuum. The energy bandwidth ΔE for the S *K*-edge measurement is only about 20 eV. It is noted that an illuminated length on the bent crystal decreases with photon energy at fixed acceptance angle of the beamline which is limited by the 5 mrad opening angle of the mask in the front-end. A wider energy bandwidth for light-element measurements can be obtained when a smaller radius of curvature is used. There is a limitation to measuring *K*-edge XANES spectra of heavy elements with this beamline because the photon flux from the light source reduces very rapidly at photon energies above the critical energy of the storage ring. However, Fe *K*-edge XANES spectra can still be measured using this beamline. The XANES spectrum for Fe foil, shown in Fig. 4, was measured in air.

The performance of the TRXAS end-station for time-resolved measurements was tested by measuring the Ti *K*-edge XANES spectra of a 5 µm-thick Ti foil (Fig. 5). An XANES spectrum has been successfully recorded using a data-acquisition speed of 25 ms. However, as can be seen in Fig. 5, the spectrum shows a poor signal-to-noise (S/N) ratio. The S/N ratio can be improved by increasing the integration time. It was found that XAS spectra with a good S/N ratio could be obtained when the integration time is 200 ms or longer, as shown in Fig. 5. Typical exposure times are between 500 ms and a few seconds. The exposure time required to saturate the detector was estimated from the measured readout voltage of the detector. It was found that, at 100 mA of a stored electron beam, the exposure times required to saturate the detector were about 2.6 s and 44 s at photon energy ranges around 2.7 keV and 7.1 keV, respectively.

Increasing the number of readouts to average is another way to improve the S/N ratio. Fig. 6 shows Ti *K*-edge XANES spectra measured using a constant total data-acquisition time of 1000 ms with different combinations of integration time and number of readouts. It can be seen from the figure that the quality of the spectra is similar for every combination. This suggests that the reduction of noise by averaging is also useful for XANES measurement using an NMOS linear image sensor.

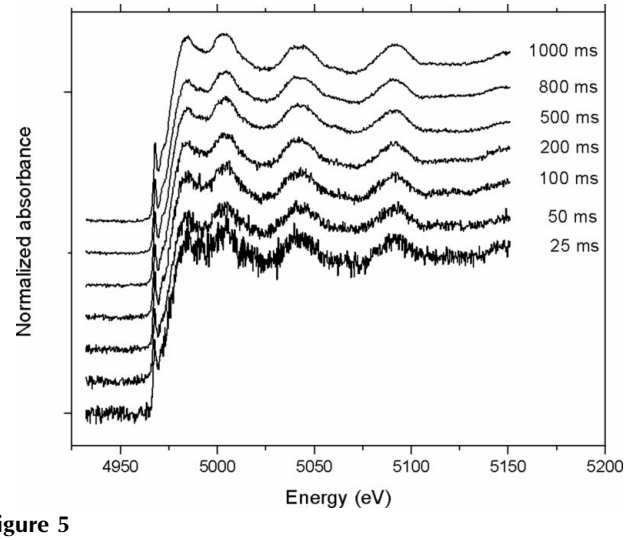

Figure 5
Normalized Ti *K*-edge XANES spectra for a 5 µm-thick Ti foil measured using integration times of 25, 50, 100, 200, 500, 800 and 1000 ms.

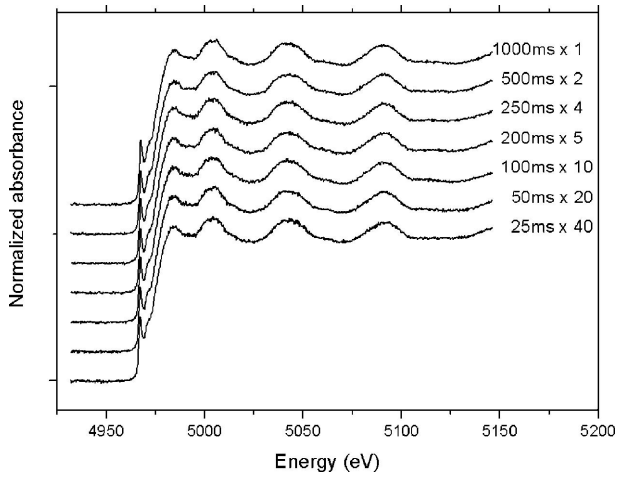

Figure 6
Normalized Ti *K*-edge XANES spectra for a 5 µm-thick Ti foil measured with a constant time resolution of 1000 ms. The measurements were made using different combinations of integration times and number of readouts to average.

4.2. *In situ* XANES measurement of TiO_2 phase transformation

TiO_2 is a useful material for many applications. It is commonly used as a white pigment in paint, plastic and paper. Because of the high reflective index, the compound is useful as an anti-reflection coating in silicon solar cells and in many thin-film optical devices (Macleod, 1986). Moreover, the compound was successfully utilized as a material for a gas sensor (Dutta *et al.*, 1999). TiO_2 has extensively been investigated and its XANES spectra are well characterized (Ruiz-López & Muñoz-Páez, 1991; Farges *et al.*, 1997; Chen *et al.*, 1997). Thus TiO_2 was chosen for testing the performance of the beamline.

There are three main polymorphs of TiO_2 found in nature; namely, anatase (tetragonal), brookite (orthorhombic) and rutile (tetragonal) which is the most stable phase of TiO_2, although only the anatase and the rutile phases are used in most applications. It is known that the optical and electrical properties of the anatase and the rutile phases are different. Thus, it is possible to engineer optical or electrical properties of this compound by controlling the ratio between the two phases. In this work, TiO_2 powder was prepared by the sol–gel method (Niltharach *et al.*, 2012). The *in situ* XANES measurement under a calcination condition was performed to monitor the formation of anatase TiO_2.

4.2.1. *In situ* cell design. Varieties of *in situ* cells for even flow through or batch processes have been used for time-resolved XAS experiments in different synchrotron radiation facilities. Some common components for these cells are heaters for the sample heating and X-ray windows made from

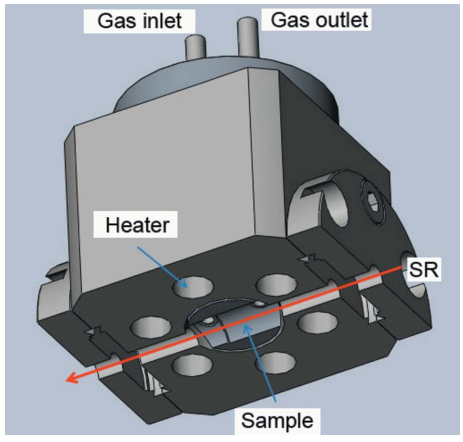

Figure 7
Cross section of the *in situ* cell for time-resolved XAS experiments at the TRXAS beamline at the SLRI. The cell is equipped with six cartridge heaters allowing the temperature to be raised to 723 K. Reactive gas can be fed through the cell while heating using the gas inlet and outlet.

Be, Al or Kapton foils for keeping the atmosphere inside the cell. In this work an *in situ* cell was developed in-house for experiments which require a thermal treatment during the measurements. The design of the cell is illustrated in Fig. 7. The dimension of the cell is 40 mm × 38 mm × 60 mm and it is made from stainless steel. A sample is put in the center of a 4 mm-diameter hole which is drilled through the cell. The cell is designed to accept the beam with a typical beam size used of 1 mm horizontally and 2 mm vertically. To maintain the inside atmosphere, two mica windows are placed at either side of the hole. Six cartridge heaters of outer diameter 6.35 mm and length 50.8 mm with K-type thermocouples are used for sample heating. The temperature of the sample is controlled by a Eurotherm 2216e temperature controller with an in-house-developed software. The *in situ* cell can be operated in the temperature range between room temperature and 723 K. Further development is required to increase the maximum temperature of the cell. The cell is installed on a three-axis linear translation stage which allows a precise alignment of the cell.

4.2.2. TiO_2 preparation. The TiO_2 powder was prepared using the sol–gel method (Niltharach *et al.*, 2012). A mixture of 0.01 mol of titanium(IV) isopropoxide (Aldrich, Technical grade), 0.26 mol of 2-propanol (Qrëc, 99.7%) and 0.07 mol of ethylene glycol (Fluka, 98.0%) was stirred at room temperature for 15 min to obtain a homogeneous solution. After that, 0.04 mol of distilled water was added to the mixture and the solution was stirred until it was clear. The solution was then aged in an oven at 348 K for 24 h such that it became a gel. The gel was subsequently dried at 383 K and calcined at 473 K using a heating rate of 1.7 K min^{-1}. The calcination was performed in a 70%-N_2/30%-O_2 gas mixture with a total flow rate of 100 cm^3 min^{-1} for 4 h to eliminate some of the organic compounds introduced by the sol–gel process. The obtained powder is mainly TiO_2. A mixed phase of anatase and rutile phase is expected when the compound is calcined at higher temperatures. The powder was pressed into a pellet 4 mm in diameter and less than 1 mm in thickness for the XAS measurement.

4.2.3. *In situ* XANES measurement. XANES spectra of TiO_2 have been extensively studied (Ruiz-López & Muñoz-Páez, 1991; Farges *et al.*, 1997; Chen *et al.*, 1997) and the amorphous to anatase transformation for TiO_2 occurs within the operating temperatures of our in-house-developed *in-situ* cell, thus the phase transformation was chosen to test the capability to perform an *in situ* measurement at the TRXAS beamline. The prepared sample was put into the *in situ* cell and heated using a heating rate of 2 K min^{-1} from room temperature to 723 K. The calcination was performed in a 70%-N_2/30%-O_2 gas mixture with a total flow rate of 100 cm^3 min^{-1}. Ti *K*-edge XANES spectra were recorded at room temperature and then every 50 K between 323 K and 573 K. From 573 K to 723 K where the phase transformation is expected, the spectra were recorded in 10 K intervals. The same temperature points during cooling were also measured. The integration time was chosen to be 200 ms and each spectrum was an average of ten readouts.

Fig. 8 shows normalized Ti *K*-edge XANES spectra of a sol–gel TiO_2 sample demonstrating a phase transition caused by the temperature change. XANES spectra of the standard anatase and rutile TiO_2 were also taken and are shown in the figure for comparison. The XANES spectra of the anatase and rutile phases have been qualitative identified (Ruiz-López & Muñoz-Páez, 1991; Farges *et al.*, 1997; Chen *et al.*, 1997). The origin of the pre-edge peaks (A_1–A_3), a characteristic shoulder (B) and main-edge peaks (C_1–C_3) was described by Farges *et al.* (1997). As seen from the standard anatase and rutile spectra, both spectra show three pre-peaks (A_1–A_3) in the energy range from 4965 to 4975 eV which correspond to

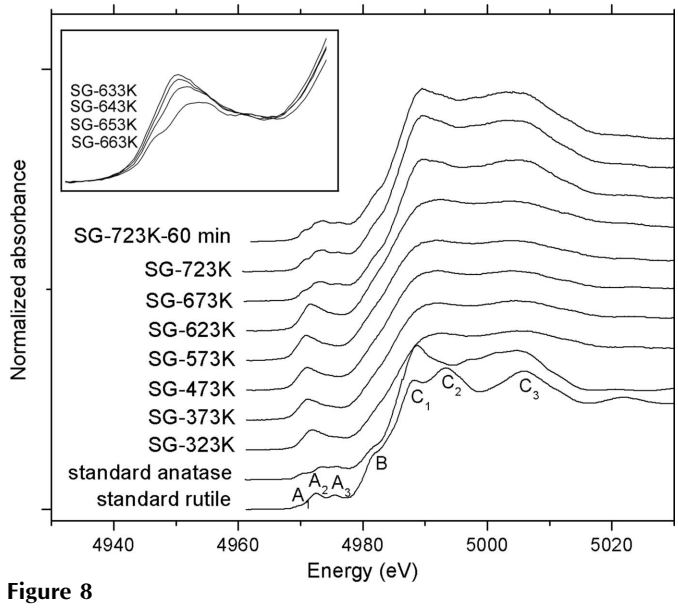

Figure 8
Normalized Ti *K*-edge XANES spectra for TiO_2 powder measured at room temperature, 373 K, 473 K, 573 K, 623 K, 673 K and 723 K during heating. Also shown are the reference spectra for the anatase and rutile phases measured at room temperature. The inset figure shows the pre-edge peaks of the Ti *K*-edge XANES spectra taken at 633 K, 643 K, 653 K and 663 K.

the $1s \rightarrow 3d$ transitions. The A_1 peak is attributed mainly to the quadrupole transitions to the t_{2g} levels in the TiO_6 octahedron while the A_2 and the A_3 peaks are attributed to the $1s$ to $3d$ dipole transitions and are designated as $1s \rightarrow t_{2g}$ and $1s \rightarrow e_g$ transitions in an octahedral field, respectively. The shoulder B is a signature of an edge-sharing structure of TiO_6 units. The main peaks (C_1–C_3) are related to transitions of excited core or valence electrons. The C_1 and C_2 peaks involve the non-bonding O $2p \rightarrow$ Ti $3d$ transition while the C_3 peak represents the transition from the bonding and anti-bonding O $2p$ orbitals. As the symmetry of the anatase and rutile phases are different (Ruiz-López & Muñoz-Páez, 1991), the relative intensities between the C_1, C_2 and C_3 peaks could be used to identify the phases. From Fig. 8 the amorphous to anatase transformation occurs at a temperature between 623 K and 673 K. It is noted that this experiment was carried out when the data acquisition software was not fully developed; some operations were done manually. This prevented us from obtaining the expected ultimate time resolution for this experiment, which is 2 s. Thus, a low heating rate of 2 K min^{-1} in the calcination process was used to monitor the transition from amorphous to anatase. The inset of Fig. 8 shows that it is possible to observe the gradual changes of the pre-edge peaks when the temperature was varied from 633 K to 663 K with a 10 K interval, indicating the phase transformation from amorphous to anatase.

From the XANES spectra of the sol–gel sample at selected temperatures shown in Fig. 8, the A_1 peak and the shoulder B are not clearly observed which could be due to the distortion from an ideal TiO_6, a partial amorphous phase at low temperatures (Purans *et al.*, 2001) or incomplete TiO_2 composition as there could still be residual organic precursors from the sol–gel process. When the temperature was raised to 673 K, the measured XANES spectrum showed all the features corresponding to the crystalline anatase phase. These features remain stable when the temperature was further increased to 723 K or holding at 723 K for 60 min which suggests that the structure of TiO_2 becomes anatase when it is calcined at 673 K and the anatase phase remains up to 723 K. The C_2 peak, characteristic of the rutile phase, was not clearly observed in any of the spectra. This indicates that a complete anatase to rutile phase transformation requires a higher calcination temperature. A mixed anatase and rutile phase has been observed at 823 K with an anatase to rutile ratio of 79:21 (Niltharach *et al.*, 2012). Fig. 9 shows the normalized Ti *K*-edge XANES spectra measured during cooling showing no significant change from the spectrum measured at 723 K which suggests that the acquired phase is stable.

5. Conclusions

A time-resolved XAS beamline has been successfully constructed at the SLRI. By using an energy-dispersive scheme, with a 1024-element photodiode array NMOS linear image sensor, a shortest data acquisition time of 25 ms for Ti *K*-edge XANES spectra was demonstrated. An in-house *in situ* cell has been developed and tested at the TRXAS beamline to observe the change in the XANES spectra during thermal treatment. Thermal treatment in the production of TiO_2 by the sol–gel method was selected as an *in situ* example experiment. The XANES spectra measured during the heating process show a clear formation of the anatase structure. The complete anatase to rutile phase transformation was not observed at 723 K.

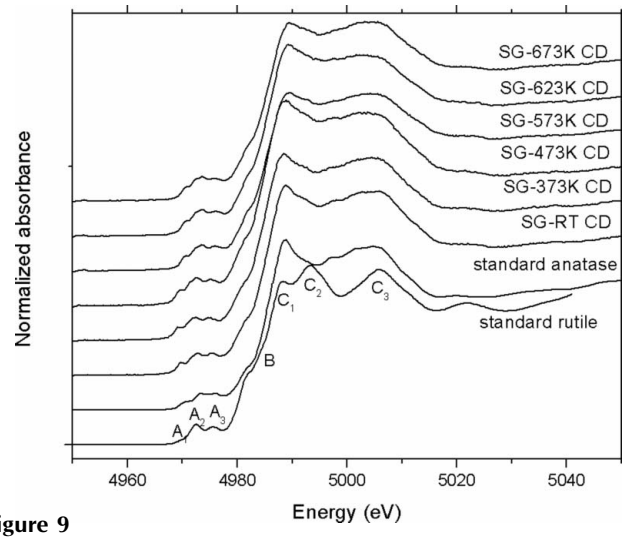

Figure 9
Normalized Ti *K*-edge XANES spectra for TiO_2 powder measured at room temperature, 373 K, 473 K, 573 K, 623 K and 673 K during cooling. Also shown are the standard spectra for the anatase and rutile phases measured at room temperature.

The authors would like to thank S. Duangnil, D. Bamroongkoh, A. Tong-orn and the Technical and Engineering Division staff for their technical assistance. WS and SC would like to acknowledge the SLRI for financial support.

References

Blank, H., Neff, B., Steil, St. & Hormes, J. (1992). *Rev. Sci. Instrum.* **63**, 1334–1337.
Bunker, G. (2010). *Introduction to XAFS: A Practical Guide to X-ray Absorption Fine Structure Spectroscopy*. New York: Cambridge University Press.
Caliebe, W. A., So, I., Lenhard, A. & Siddons, D. P. (2006). *Radiat. Phys. Chem.* **75**, 1962–1965.
Cezar, J. C., Souza-Neto, N. M., Piamonteze, C., Tamura, E., Garcia, F., Carvalho, E. J., Neueschwander, R. T., Ramos, A. Y., Tolentino, H. C. N., Caneiro, A., Massa, N. E., Martinez-Lope, M. J., Alonso, J. A. & Itié, J.-P. (2010). *J. Synchrotron Rad.* **17**, 93–102.
Chen, J., Zhang, H., Tomov, I. V., Ding, X. & Rentzepis, P. M. (2007). *Chem. Phys. Lett.* **437**, 50–55.
Chen, L. X., Lee, P. L., Gosztola, D. J., Svec, W. A. & Wasielewski, M. R. (1999). *J. Synchrotron Rad.* **6**, 403–405.
Chen, L. X., Rajh, T., Wang, Z. & Thurnauer, M. C. (1997). *J. Phys. Chem. B*, **101**, 10688–10697.
Couves, J. W., Thomas, J. M., Catlow, C. R. A., Greaves, G. N., Baker, G. & Dent, A. J. (1990). *J. Phys. Chem.* **94**, 6517–6519.
Dartyge, E., Depautex, C., Dubuisson, J. M., Fontaine, A., Jucha, A., Leboucher, P. & Tourillon, G. (1986). *Nucl. Instrum. Methods Phys. Res. A*, **246**, 452–460.
Dutta, P. K., Ginwalla, A., Hogg, B., Patton, B. R., Chwieroth, B., Liang, Z., Gouma, P., Mills, M. & Akbar, S. (1999). *J. Phys. Chem. B*, **103**, 4412–4422.

Farges, F., Brown, G. E. & Rehr, J. J. (1997). *Phys. Rev. B*, **56**, 1809–1819.
Flank, A. M., Fontaine, A., Jucha, A., Lemonnier, M., Raoux, D. & Williams, C. (1983). *Nucl. Instrum. Methods Phys. Res.* **208**, 651–654.
Fontaine, A., Dartyge, E., Jucha, A. & Tourillon, G. (1987). *Nucl. Instrum. Methods Phys. Res. A*, **253**, 519–522.
Hedman, B. & Pianetta, P. (2007). *AIP Conf. Proc.*, **882**, 1–937.
Koningsberger, D. C. & Prins, R. (1988). Editors. *Principles, Applications, Techniques of EXAFS, SEXAFS and XANES. Chemical Analysis: A Series of Monographs on Analytical Chemistry and its Applications*, Vol. 92. Toronto: Wiley-Interscience.
Lützenkirchen-Hecht, D., Grundmann, S. & Frahm, R. (2001). *J. Synchrotron Rad.* **8**, 6–9.
Macleod, H. A. (1986). *Thin Film Optical Filters*, p. 370. New York: MacMillan.
Meneses, C. T., Flores, W. H., Sotero, A. P., Tamura, E., Garcia, F. & Sasaki, J. M. (2006). *J. Synchrotron Rad.* **13**, 468–470.
Niltharach, A., Kityakarn, S., Worayingyong, A., T-Thienprasert, J., Klysubun, W., Songsiriritthigul, P. & Limpijumnong, S. (2012). *Physica B*, **407**, 2915–2918.
Pascarelli, S., Neisius, T., De Panfilis, S., Bonfim, M., Pizzini, S., Mackay, K., David, S., Fontaine, A., San Miguel, A., Itié, J. P., Gauthier, M. & Polian, A. (1999). *J. Synchrotron Rad.* **6**, 146–148.
Purans, J., Azens, A. & Granqvist, C. G. (2001). *Electrochim. Acta*, **46**, 2055–2058.
Ruiz-López, M. F. & Muñoz-Páez, A. (1991). *J. Phys. Condens. Matter*, **3**, 8981–8990.
Tassell, C. & Maule, D. J. (1979). *Microelectron. J.* **10**, 35–44.